Materials Today Communications 29 (2021) 102781

Contents lists available at ScienceDirect

Materials Today Communications

journal homepage: www.elsevier.com/locate/mtcomm

Transport and photophysical studies on porphyrin-containing sulfonated poly(etheretherketone) composite membranes

Joana F.M. Sousa [a], João Pina [a], Carla Gomes [a], Lucas D. Dias [a,b], Mariette M. Pereira [a], Dina Murtinho [a], Paula Dias [c], João Azevedo [c], Adélio Mendes [c], J. Sérgio Seixas de Melo [a], Alberto A.C.C. Pais [a], Marta Pineiro [a,*], Artur J.M. Valente [a,*]

[a] University of Coimbra, CQC, Department of Chemistry, 3004-535 Coimbra, Portugal
[b] São Carlos Institute of Physics, University of São Paulo, 13566-590 São Carlos, Brazil
[c] LEPABE - Laboratory for Process Engineering, Environment, Biotechnology and Energy, Faculty of Engineering, University of Porto, Rua Dr. Roberto Frias, 4200-465 Porto, Portugal

ARTICLE INFO

Keywords:
SPEEK
Porphyrins
Nafion
Redox flow batteries
Transport properties

ABSTRACT

The development of efficient and reliable membranes for redox flow batteries (RFBs) with high ionic conductivity and selectivity is challenging. Aiming the development of better membranes, we have synthesized porphyrin-containing sulfonated poly(etheretherketone) (SPEEK). In particular, the effect of water soluble 5,10,15,20-*tetrakis*(*N*-methyl-4-pyridinyl)porphyrin iodide ($TMePyPI_4$) and its Cu(II) complex, 5,10,15,20-*tetrakis*(*N*-methyl-4-pyridinyl)porphyrinate copper(II) iodide, ($CuTMePyPI_4$), at 0.1–0.3 wt%, have been assessed. Photophysical studies have shown that porphyrins are aggregated in the J-type. The obtained composite membranes show high macroscopic homogeneity and lower ability to sorb water when compared with pristine SPEEK membranes but comparable protonic conductivity. The hydronium diffusion and permeability coefficients suggest that at low porphyrin concentrations an enhancement of proton channels occurs, whilst at high concentration that effect decreases due to the formation of porphyrin aggregates. A similar effect occurs in the permeation of vanadium ions through composite membranes with a remarkable lower permeability and diffusion coefficients when compared with those obtained for Nafion 115 membranes. This along with the improved thermal stability of porphyrin-containing SPEEK composite membranes indicate that these advanced materials can be used for improving the performance of RFBs.

1. Introduction

The concentration of carbon dioxide (CO_2) in the atmosphere caused by extensive use of fossil fuel combustion has become one of the main environmental challenges. Sustainable strategies for decreasing the atmospheric CO_2 concentration are urgent. Solutions can be reached by using environmentally friendly routes to generate electricity from renewable energy sources, such as wind and solar, and to convert CO_2 into value added chemicals (ethanol, methanol, *etc.*). The implementation of any of those solutions depends on the ongoing development of energy conversion and storage technologies, such as redox flow batteries or fuel cells. Fuel cells are electrochemical systems with high efficiency for hydrogen-based energy conversion; however, when methanol or ethanol are used as alternative fuels there is a significant reduction in performance [1,2]. Redox flow batteries (RFBs) are considered one of the most suitable technologies for stationary applications. RFBs are characterized by its ability for reversible conversion between chemical and electrical energies based on two redox reactions. For that reason, RFBs are denominated as regenerative fuel cells, as energy is stored in incoming fuels, in the form of two redox pairs dissolved in liquid electrolytes, which are easily and efficiently convertible into electricity. This technology handles power and storage capacity separately; the power is related to the size of the electrochemical cells stack, while the capacity is related to the size of the tanks storing the electrolytes. Other properties related with the viscosity and composition may also play an important role [3,4].

The proton exchange membrane (PEM) is a key component influencing performance, durability and cost of RFB and fuel cells. The membrane has two essential functions, transfer protons from the anode to the cathode and act as barrier to the passage of electrons, gas and

* Correspondence to: Department of Chemistry, University of Coimbra, 3004-535 Coimbra, Portugal.
E-mail addresses: mpineiro@qui.uc.pt (M. Pineiro), avalente@ci.uc.pt (A.J.M. Valente).

https://doi.org/10.1016/j.mtcomm.2021.102781
Received 21 July 2021; Received in revised form 7 September 2021; Accepted 8 September 2021
Available online 13 September 2021

electrolytes between the electrodes [5]. Nafion, developed by DuPont, is one of the most common and commercially available PEMs as it is standard for electrochemical reactions; it shows a remarkable proton conductivity, good thermal, mechanical and chemical stability, and has been, so far, the most used polymer in high-performance fuel applications [6]. These membranes allow only protons to crossover (cation exchange) and are available with various thicknesses. However, the high cost and high crossover rate are important drawbacks, which limits efficiency of RFB. Thus, the development of proton exchange membranes to overcome those drawbacks is an active research topic in the development of clean technology for energy production and storage [7,8].

Sulfonated poly(etheretherketone) (SPEEK) membranes are a reliable and effective alternative to Nafion as a consequence of its better thermal stability, low cost and acceptable proton conductivity [9–11]; additionally there are evidences that they display lower crossover when compared with Nafion [12]. One of the strategies followed to improve the performance of the SPEEK-based membranes has been to load them with different nanofillers, including carbon nanotubes and graphene oxide [13–15], silsesquioxane derivatives [16] and zirconium phosphate nanosheets [17].

Porphyrins and their metal complexes are key molecules for promoting the development of new material in a wide range of applications, including solar energy conversion and carbon dioxide reduction [18, 19]. Porphyrins have been applied in composite SPEEK membranes to improve the charge transport [20] and the proton conductivity [21]. Furthermore, due to their ability to self-aggregate [22], porphyrins can modify the physical-chemical properties of the polymeric membrane.

Recently, porphyrin-containing SPEEK membranes were synthesized and characterized [21,23]. Carbone et al. showed that the presence of 5, 10,15,20-tetrakis(4-pyridyl)porphyrin (TPyP) into SPEEK membranes, in particular for the composite membrane containing 0.77 wt% TPyP, contributed to better power density, tested in a proton exchange fuel cell, when compared with the pristine SPEEK membrane [23]; more recently, the same authors assessed the performance of *meso*-tetrakis (4-sulfonatophenyl)porphyrin (TPPS)-containing SPEEK composite membranes [21]. Previous studies showed that weak self-aggregation and high photothermal stability of Cu complexes are beneficial for stabilizing the polymer on polymer solar cells [24] and to improve the thermal stability of perovskite solar cells [25].

In this work, we report a thorough study involving physical-chemical, electrochemical and photophysical analysis of SPEEK-based composite membranes containing two water soluble porphyrins: 5,10,15,20-*tetrakis*(*N-methyl-4-pyridinyl*)porphyrin iodide ($TMePyPI_4$) and its copper complexes, 5,10,15,20-*tetrakis*(*N-methyl-4-pyridinyl*)porphyrinate copper(II) iodide, ($CuTMePyPI_4$). Copper complex of water-soluble porphyrin was introduced to control aggregation and modify the properties of SPEEK, showing good mass transport properties and high thermal and chemical stability.

2. Experimental

2.1. Materials

Pyrrole, 4-pyridinecarboxaldehyde, propionic acid, nitrobenzene, methyl iodide, copper(II) acetate monohydrate, vanadium(IV) oxide sulfate hydrate (97%) and poly(oxy-1,4-phenyleneoxy-1,4-phenylenecarbonyl-1,4-phenylene) (PEEK), Sephadex G-10 Medium were purchased from Sigma-Aldrich and used as received. Sulfuric acid (96%, Honeywell/Fluka™) and hydrochloric acid (Fisher scientific) were used for PEEK sulfonation and HCl permeation, respectively. *N,N*-Dimethylformamide, was used as solvent for membrane casting and was supplied from Merck. Commercial membranes of Nafion 115 (127 μm) were acquired from Sigma.

2.2. Synthesis of porphyrins

Synthesis under microwave irradiation were performed using a CEM Discover S-Class microwave reactor with automated control of power, temperature and pressure.

Ball milling reactions were performed in a Retsch MM 400 with constant frequency and time monitoring. Steel jars (10 mL) and balls (7 mm diameter). HPLC Elite Lachrom HPLC-DAD system with L-2455 Diode Array Detector, L-23000 Column Oven (RP-18 endcapped column - 5 μm) from Merck), L-2130 Pump and a L-2200 Auto Sampler. NMR spectra were registered at room temperature (RT) in a Bruker Avance III spectrometer, operating at 400 MHz. TMS was the internal standard used. Chemical shifts (δ) and coupling constants (J) are indicated in ppm and Hz, respectively.

2.2.1. 5,10,15,20-tetrakis(4-pyridyl)porphyrin, TPyP

The porphyrin was synthesised using previously described microwave-assisted methodology and purified through column chromatography followed by recrystallization [26].

2.2.2. 5,10,15,20-tetrakis(4-pyridyl)porphyrin, TPyP

Yield: 15%, 928 mg (dark-purple solid); mp (ºC) > 300; UV-Vis (CH_2Cl_2): λmax, nm (relative absorbance, %) = 415 (100), 510.5 (7.7), 544 (3.7), 585.5 (3.9), 641.5 (2.7); ^{1}H NMR (400 MHz, $CDCl_3$): δ, ppm = 9.07 (8 H, d, J = 4.2 Hz), 8.87 (8 H, s), 8.16 (8 H, d, J = 4.2 Hz), − 2.92 (2 H, bs). Data in accordance with previous report [26].

2.2.3. 5,10,15,20-tetrakis(N-methyl-4-pyridinyl)porphyrin iodide, $TMePyPI_4$

Tetramethyl pyridinyl cationic porphyrin was synthesized through previously described methodology [26]. The reaction product was analysed by HPLC-DAD using as stationary phase Purospher® STAR RP-18 endcapped (5 μm) and as eluent: potassium acetate (pH = 3)(A) and MeCN:H_2O (50:50)(B) (from 100:0–30:70(A/B v/v)); 5% increment of B each min. for 12 min; 5% increment of B each 2 min until 22 min and 30:70 (A/B v/v) ratio for 12 min. Flow rate of 0.8 mL/min in the first 9 min and then 0.4 mL/min until 35 min. L-2455 Diode Array Detector (400 nm). Percentage of total chromatogram integration at retention time 13.7 min, relative area 98%.

2.2.4. 5,10,15,20-tetrakis(N-methyl-4-pyridinyl)porphyrin tetraiodine, $TMePyPI_4$

Yield: 94%, 270 mg (dark-purple solid); mp (ºC) > 300; UV-Vis (H_2O): λ_{max}, nm (relative absorbance, %) = 422 (100), 518 (8.8), 553.5 (4.7), 586 (5), 637.5 (2.9); ^{1}H NMR (400 MHz, (d^6-DMSO): δ, ppm = 9.51 (8 H, d, J = 6.8 Hz), 9.22 (8 H, s), 9.01 (8 H, d, J = 6.8 Hz), 4.74 (12 H, s), − 3.09 (2 H, bs). Data in accordance with previous report [26].

2.2.5. 5,10,15,20-tetrakis(N-methyl-4-pyridinyl)porphyrinate copper(II) iodide, $CuTMePyPI_4$

A mixture of 5,10,15,20-*tetrakis*(*N*-methyl-4-pyridyl)porphyrin (50 mg, 0.042 mmol), copper(II) acetate monohydrate (10 equiv, 84.2 mg) and two steel spheres were placed in steel jar and submitted to mechanical action in a ball milling system (Retsch 400 MM) at 25 Hz during 90 min. The reaction product was purified through sephadex G-10 filtration column, using water as eluent. The metalloporphyrin was collected and evaporated under reduced pressure. HPLC-DAD analysis using as stationary phase Purospher® STAR RP-18 encamped (5 μm) and as eluent: potassium acetate (pH = 3)(A) and MeCN:H_2O (50:50)(B) (from 100:0–30:70(A/B v/v)); 5% increment of B each min. for 12 min; 5% increment of B each 2 min until 22 min and 30:70 (A/B v/v) ratio for 12 min. Flow rate of 0.8 mL/min in the first 9 min and then 0.4 mL/min until 35 min. L-2455 Diode Array Detector (400 nm). Percentage of total chromatogram integration at retention time 14.2 min relative area 98%.

5,10,15,20-*tetrakis*(*N-methyl-4-pyridinyl*)porphyrinate copper(II) iodide, **$CuTMePyPI_4$,** Yield: 46%, 24.3 mg (dark-purple solid); mp (ºC) >

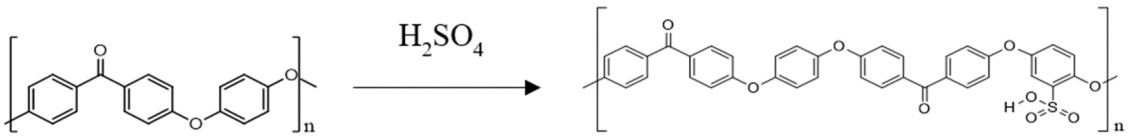

Scheme 1. .

300; UV-Vis (H_2O): λ_{max}, nm (relative absorbance, %) = 425 (100), 548 (15.6).

2.3. Sulfonation of PEEK

PEEK particles were first dried at 100 ºC overnight. Then 6 g of PEEK was dissolved gradually in 120 mL of concentrated H_2SO_4 (96 wt%) under stirring (400 rpm), at RT, during about 5 days. The sulfonation reaction (Scheme 1) is worked up according to the procedure previously described [10]. After that, the polymer was dried at 45 ºC for 1 day and the degree of sulfonation was measured through ^{1}H NMR (Bruker BiospinGmbH 400 MHz) using DMSO-d_6 (Sigma) as solvent. A sulfonation degree of 63% has been found.

2.4. Composite membranes

The sulfonated PEEK (SPEEK) was further used as a matrix membrane for porphyrin incorporation. The membranes have been prepared as follows: the SPEEK (10% (w/v)) was initially dissolved in dimethylformamide (DMF) solvent, at RT. After that, DMF solutions of 5,10,15,20-*tetrakis*(*N*-methyl-4-pyridinyl)porphyrin iodide ($TMePyPI_4$) and 5,10,15,20-*tetrakis*(*N*-methyl-4-pyridinyl)porphyrinate copper(II) iodide, ($CuTMePyPI_4$), previously prepared, were added to SPEEK solutions. The concentrations of porphyrin and SPEEK in the blend solution are 0.1 wt%, 0.2 wt% and 0.3 wt% [23]. The membranes were prepared by casting using an Elcometer (K4340M11) automatic film applicator. The obtained membranes are then activated by immersing in a 1 M H_2SO_4 aqueous solution during 24 h. Then the membranes are soaked in water to remove the H_2SO_4 in excess.

2.5. Characterization of composite membranes

The incorporation of porphyrin into SPEEK has been evaluated by attenuated total reflectance - Fourier transform infrared (ATR-FTIR) spectroscopy, using a Varian Cary 630 FTIR spectrometer. The surface morphologies of blend films were analyzed by scanning electron microscopy (SEM). SEM images were recorded on a JSM 6010LV/6010LA, Jeol (Tokyo, Japan) scanning microscope, microscope operating under low vacuum, using a 10 kV potential.

Thermogravimetric analysis (TGA) were performed in a TG209 F3 Tarsus thermogravimetric analyzer (Netzsch Instruments). Samples (*ca.* 5 mg) were weighed in alumina crucibles and heated from 30 ºC to 900 ºC, at a heating rate of 10 ºC/min, under N_2 atmosphere (flow rate of 20 mL/min).

Water uptake measurements are used for the assessment of the hydrophilic/hydrophobic balance occurring as a function of blend composition. Four replicates (*ca.* 1 ×1 cm) of each membrane were taken and weighted (w_{dry}). Then, membranes were soaked in Milli-Q water for 6 days, at RT. After that, the soaked membranes were weighed (w_{wet}). The water uptake (H_p) was calculated by:

$$H_P(\%) = \frac{w_{wet} - w_{dry}}{w_{dry}} \times 100 \quad (1)$$

2.6. Transport properties

Three different types of transport properties have been measured: electrical conductance, proton conductivity and the diffusion and permeation of HCl through SPEEK-based membranes.

The bulk resistivity (ρ_b) of membranes was computed through the equation:

$$\rho_b = 2\pi sR \quad (2)$$

where s is the probe spacing (0.1221 cm) and R is the electrical resistance of the sample, measured by using a four probe electrode (HL Jandel), coupled to a Keithley 2401 SourceMeter.

The proton conductivity (σ) was obtained through electrochemical impedance spectroscopy (EIS) measured in 0.5 M H_2SO_4 and using an Autolab/PGSTAT302N workstation controlled by Nova software package (Nova version 1.11). All membranes were measured at open circuit potential (OCP) in a frequency range of 200 kHz to 10 Hz. Two platinum wires were used as electrodes (placed close to the membrane). The area of the membranes was 4 cm^2.

The ability of membranes for proton permeability and the concentration of free hydrogen ions in the polymer phase have been assessed by measuring the flux of HCl, using a cell similar to that reported elsewhere [27] and the time-lag method. The horizontal Franz-type cell consists of two compartments with *ca.* 200 mL (V). The donor compartment is filled with aqueous 0.1 M HCl solution, and the receptor compartment, filled with water. Solutions in both compartments were kept at constant temperature at 25.0 ± 0.1 ºC by using a Velp Sientifica Multistirrer 6 thermostat. The flux of HCl (from the donor to the receptor compartments) is quantified by measuring the electrical conductivity (κ) in the receptor compartment using tetracon® 325, controlled by WTW™ Multi/ACHAT II software [28]. The conductivity cell constant is calculated before each experiment. The permeability (P) and the integral diffusion (D) coefficients, and the partition coefficient (K), were computed by using Eqs. (3–5), respectively:

$$P = \frac{Vl}{A}\frac{1}{[HCl]}\frac{dc_t}{dt} \quad (3)$$

$$D = \frac{l^2}{6\theta} \quad (4)$$

$$K = \frac{P}{D} \quad (5)$$

where K is the partition coefficient (Henry's coefficient), θ is the time lag, l is the membrane thickness, A is the permeation area (3.14 cm^2) and dc_t/dt corresponds to the slope of the dependence of the flux on time, under steady-state conditions.

Vanadium permeability was also measured to evaluate the performance of the composite membrane towards crossover flow. The measurements were carried out using the same permeation cell described above. However, in this case, the donor compartment contain 1.0 M VO^{2+} in 2.0 M H_2SO_4 and the receptor compartment was filled with 2.0 M H_2SO_4 (200 mL) [29]. The flux of VO^{2+} was measured by UV–vis spectrophotometry (Shimadzu, model UV-2450) and the permeability and diffusion coefficients were computed by using Eqs. (3) and (4) by

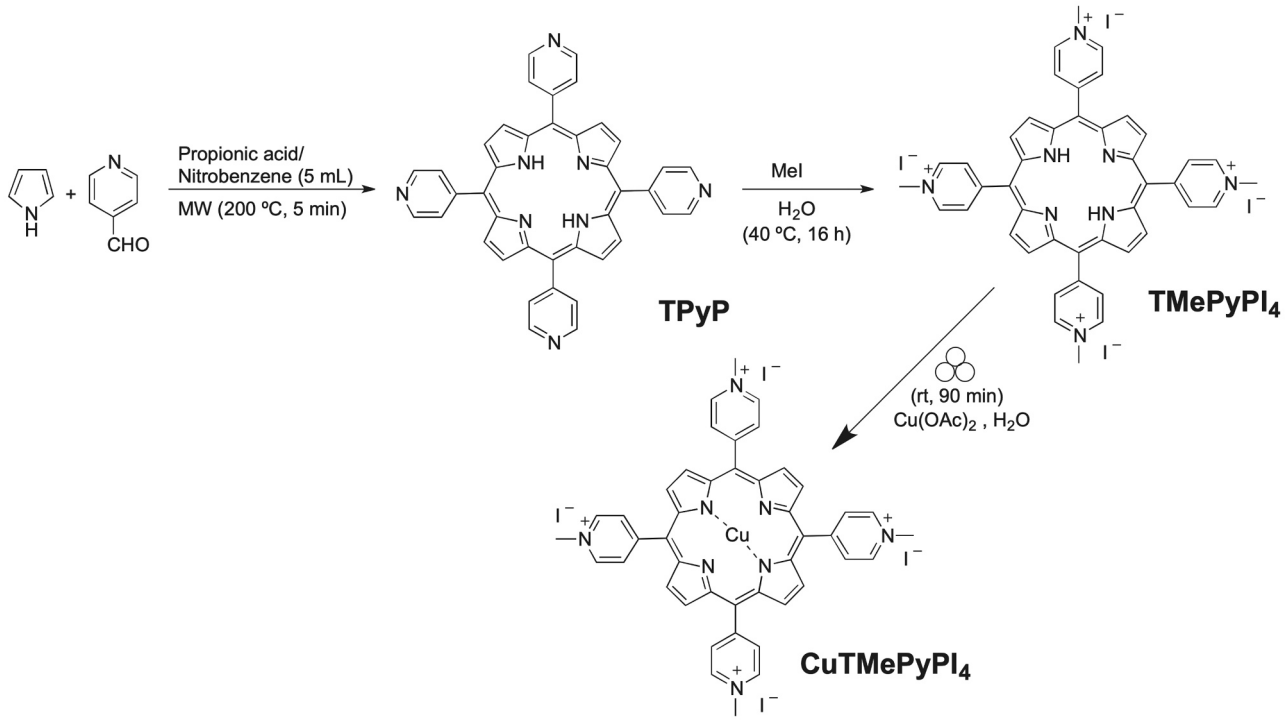

Scheme 2. Synthetic procedure and abbreviations of the cationic porphyrins in this work.

substituting [HCl] by the VO^{2+} concentration.

2.7. Photophysical characterization

The spectral data, namely the absorption and fluorescence spectra were obtained with Cary 5000 UV-Vis-NIR and Horiba-Jobin-Ivon Fluorolog 3.22 spectrometers, respectively. The emission spectra were corrected for the instrumental, namely wavelength response, of the equipment with correction factors for emission and excitation spectra. The absorption spectra of the films were recorded by collecting the spectra in the diffuse reflectance mode using a Cary 5000 UV-Vis-NIR spectrophotometer equipped with an integrating sphere (200–2500 nm range). Prior to the determination of the spectra of the films a background correction was performed by obtaining the baseline with 100% and 0% reflectance (using a polytetrafluoroethylene, PTFE, reference sample and the blocked beam, respectively). The conversion to absorption was carried out assuming the Kubelka-Munk function, F(R) [30].

The fluorescence quantum yields obtained in dimethylsulfoxide (DMSO) solution were determined by the comparative method, using tetraphenyl-porphyrin in toluene solution as standard, $\phi_F = 0.11$ [31,32]. In the solid state (films) the fluorescence quantum yields were measured using the absolute method with a Hamamatsu Quantaurus QY absolute photoluminescence quantum yield spectrometer, model C11347 (integration sphere).

Singlet oxygen yields (ϕ_Δ) were obtained by the measurement of phosphorescence emission at 1270 nm followed upon irradiation of the aerated solution of the samples in DMSO with excitation at 355 nm from a Nd:YAG laser with a setup described elsewhere [33]. 5,10,15,20-tetraphenylporphyrin in toluene ($\phi_\Delta = 0.66$) was used as standard [34] for the ϕ_Δ measurements.

Fluorescence decays were measured using a home-built picosecond time-correlated single photon counting (ps-TCSPC) apparatus described elsewhere [33].

The fluorescence decays and the instrumental response function (IRF) were collected using 1024 channels in a time scale up to 52.7 ps/channel (using a Spectra Physics frequency divider, Pulse picker model 3980–2 s, to reduce the fundamental laser repetition rate to 8 MHz). Deconvolution of the fluorescence decay curves was performed using the method of the modulation functions, as implemented in the SAND program by George Stricker [35].

Time resolved ultrafast transient absorption measurements were collected in a broadband HELIOS spectrometer (350–1600 nm) from Ultrafast Systems, described elsewhere [36]. The transient absorption data was obtained with excitation at 450 nm (and using a 450 nm centered bandpass interference filter, FWHM= 10 nm in the pump optical path) and probed in the 350–750 nm range. The measurements in solution were obtained in a 2 mm quartz cuvette, with absorptions of *ca.* 0.1 at the pump excitation wavelength. Photodegradation of the solution samples was avoided by stiring or kept in movement using a motorized translating sample holder during the experiments. Spectral chirp was corrected using Surface Xplorer PRO program from Ultrafast Systems. Global analysis of the data (using a sequential model) was made using the Glotaran software.

3. Results and discussion

3.1. Porphyrin synthesis

5,10,15,20-*tetrakis*(4-pyridyl)porphyrin, TPyP was synthesized in one-pot by condensation of pyrrole with 4-pyridylaldehyde under microwave irradiation. The water-soluble tetramethylate derivative 5,10,15,20-*tetrakis*(*N*-methyl-4-pyridinyl)porphyrin iodide, $TMePyPI_4$, Scheme 1, were synthetized accordingly to previously described methodologies [26,37,38]. The 5,10,15,20-*tetrakis*(4-pyridyl)porphyrin, TPyP was synthesized under in one-pot method by condensation of pyrrole with 4-pyridylaldehyde under microwave irradiation, followed by cationization with methyl iodide (Scheme 2).

The synthesis of the copper(II) complex was achieved *via* mechanochemistry. The water-soluble porphyrin $TMePyPI_4$ and ten equivalents of the metal salt, and two stain-steel spheres were place in the jars and submitted to mechanical action for 90 min. The metalloporphyrin was obtained with 46% yield after purification by molecular exclusion chromatography (Scheme 2).

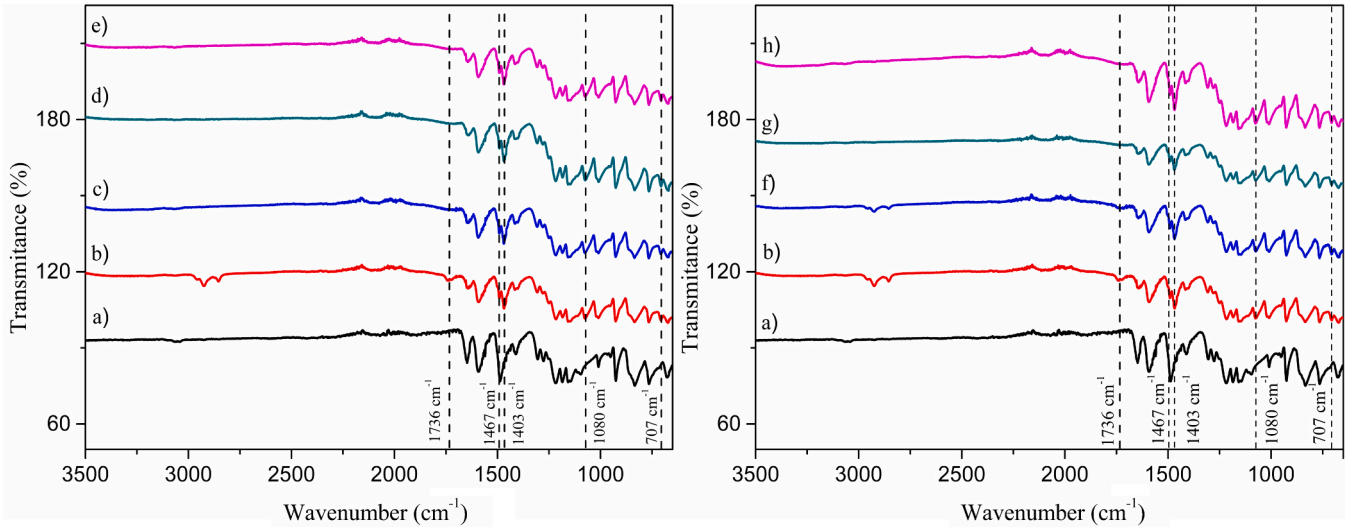

Fig. 1. FTIR spectra of PEEK (a) and SPEEK composite films without (b) and with $TMePyPI_4$ (c) 0.1%, (d) 0.2% and (e) 0.3%, and $TMePyPI_4$ (f) 0.1%, (g) 0.2% and (h) 0.3%.

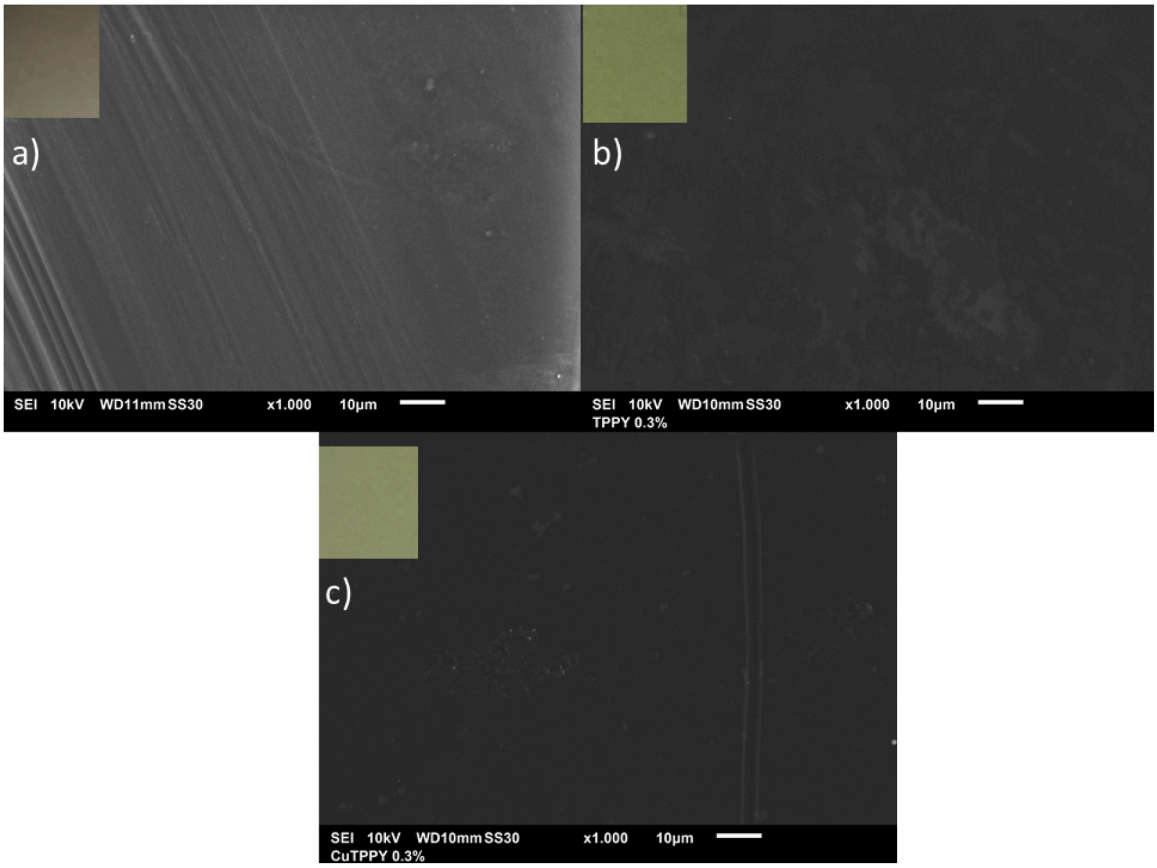

Fig. 2. SEM micrographs of: (a) SPEEK, (b) SPEEK/$TMePyPI_4$ (0.3 wt%) and (c) SPEEK/$CuTMePyPI_4$ (0.3 wt%) membranes. ×1000 magnification. Inset: photos of the corresponding membranes.

The classical methodologies for the synthesis of metaloporphyrins involve the use of large excess of metal salts and large quantities of hazardous and/or high boiling point organic solvents at high temperature for long reaction times. Therefore, the solvent-free synthesis herein described, is an alternative sustainable methodology, in agreement with the second, third, fifth and sixth principles of Green Chemistry [39].

3.2. Characterization of SPEEK-based composite membranes

Composite films of SPEEK (10% w/v) with different amounts of $TMePyPI_4$ (0.1–0.3 wt%) and $CuTMePyPI_4$ (0.1–0.3 wt%) were prepared. The sulfonation of PEEK has been assessed by FTIR (Fig. 1). Comparing both spectra it can be concluded that new bands occurring at *ca.* 1080 and 1403 cm^{-1} are assigned to symmetric and unsymmetrical

Table 1
Thermal properties of neat and SPEEK-based composite films for the observed thermal transition regions: I, II, III and IV.

	$T_{m,I}$ / °C	$T_{m,II}$ / °C	$T_{m,III}$ / °C	$T_{m,IV}$ / °C
SPEEK	70	247	317	532
SPEEK/TMePyPI$_4$ 0.1 wt%	60	267	337	522
SPEEK/TMePyPI$_4$ 0.3 wt%	65	–	332	527
SPEEK/CuTMePyPI$_4$ 0.1 wt%	81	–	332	537
SPEEK/CuTMePyPI$_4$ 0.3 wt%	86	–	332	537

stretching vibrations of sulfonate groups [40]. The peak at *ca.* 1467 cm^{-1} corresponds to the vibration mode of the aromatic C-C [41]. The peak at 1736 cm^{-1} is due to the aromatic sulfur (C═C−S) vibrational mode, as due to the linkage of sulfonic acid group to the PEEK backbone [42]. Another band that can be attributed to the sulfonic group, in particular to the S-O stretching one, can be found at *ca.* 707 cm^{-1} [12]. Upon the incorporation of porphyrins (either native or complexed with copper ion) no significant change in FTIR spectra is observed. The lack of vibrational modes characterizing the porphyrins may be related with their occurrence in films at low concentrations. However, it is worth noticing that the SPEEK band occurring at *ca.* 1736 cm^{-1} is not observed.

Despite the lack of features in FTIR analysis related with the porphyrins, which can easily be justified by its low content into the composite, it can be seen, by visual inspection, that films with porphyrins show a green translucent aspect, suggesting a macroscopic homogeneous dispersion throughout the film (see the inset photos in Fig. 2). The surface morphology micrographs show homogeneous profile (*i.e.*, no phase separation or porphyrin aggregation are occurring at surface) and featureless non-porous surface in agreement with that found by Carbone et al. for membranes of SPEEK with higher concentrations of TMePyPI$_4$ [23].

The thermal stability of the SPEEK and composites was studied using TGA. The temperature of maximum degradation rate for the transition I ($T_{m,I}$), shown in Table 1, was obtained by using the minimum in the derivative thermogravimetry (DTG) curve. SPEEK shows 4 thermal transitions (see regions I to IV in the Fig. 3): region I) occurs at 70 °C and is due to residual solvent; region III) aims at the well-defined weight loss at 317 °C that is related to desulfonation reaction of –SO_3H groups; and region IV) corresponds to the final degradation step at *ca.* 537 °C assigned to the degradation of polymer backbone [43].

Comparing with composite membranes, SPEEK membranes shows a further degradation step corresponding to $T_{m,II}$ = 247 °C (region II), which can be justified by the desorption of high melting temperature organic solvent (DMF) [44]. It can be concluded that the incorporation of porphyrins leads to a thermal stabilization of the SPEEK membranes, from 15 °C to 20 °C, which may result from an increase in the intermolecular H-bonding, resulting from SPEEK-SPEEK or SPEEK-porphyrin interactions and consequent stabilization of the protonated sulfonate groups.

3.3. Photophysical studies

In DMSO solution, the TMePyPI$_4$ and its copper derivative display the characteristic absorption of the tetraphenylporphyrin derivatives, absorption maxima of the Soret band at 426 nm and Q bands at 526 nm, 557 nm, 591 nm and 644 nm for the free-based membranes, and, Soret Band at 426 nm and Q band at 550 nm for the copper complex. In solution, the fluorescence emission spectrum of TMePyPI$_4$ shows two broad bands at *ca.* 650 nm and *ca.* 715 nm (see Fig. 5). The fluorescence emission drop with the insertion of paramagnetic copper(II) due to the exchange interaction involving the lowest triplet of the porphyrin core unit and the d_{x2-y2} unpaired electron of the metal, being undetectable in water [45] and in DMSO solution [32,46].

Going to the SPEEK films loaded with porphyrin/SPEEK 0.1% weight

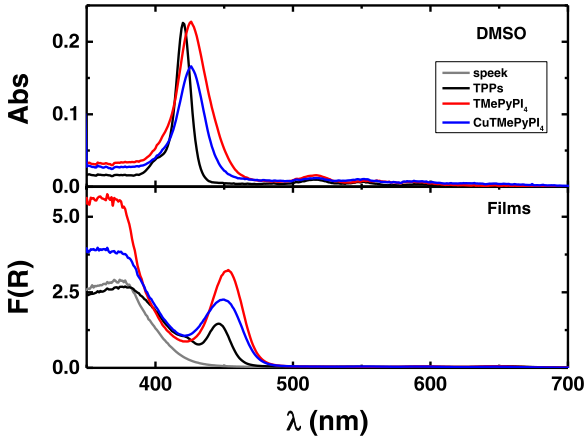

Fig. 4. UV-Vis absorption spectra for the investigated porphyrins in DMSO and loaded in SPEEK films with porphyrin/SPEEK 0.1% weight percentage ratio at 293 K.

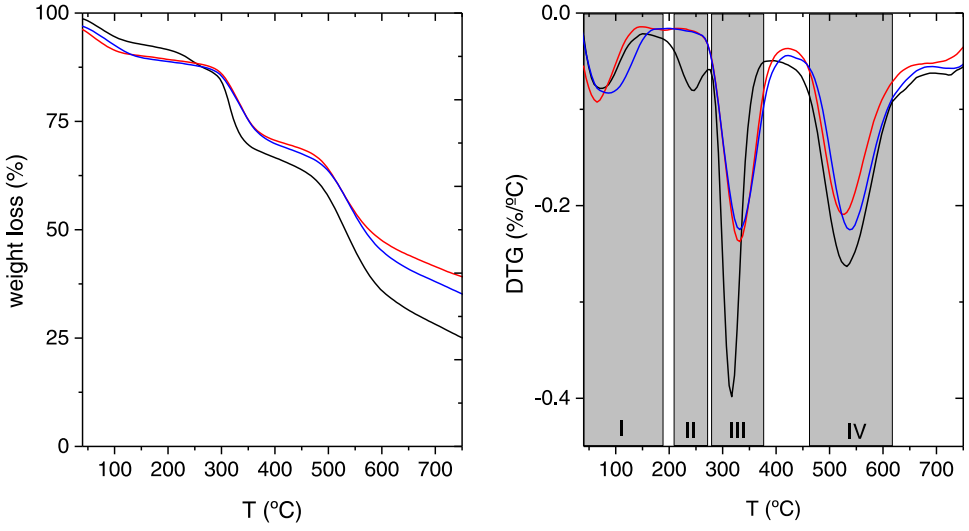

Fig. 3. TGA and corresponding DTG curves for SPEEK (black lines), SPEEK/TMePyPI$_4$ (0.3 wt%, red lines) and SPEEK/CuTMePyPI$_4$ (0.3 wt%, blue lines). For the meaning of I-IV regions see the text.

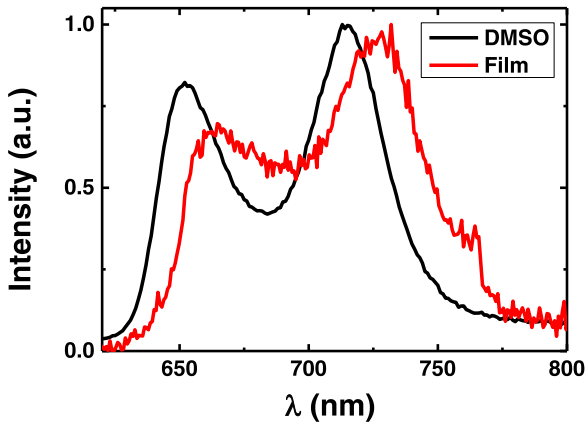

Fig. 5. Normalized fluorescence emission spectra for porphyrin $TMePyI_4$ obtained in DMSO and dispersed in SPEEK films with porphyrin/SPEEK 0.1% weight percentage ratio at T = 293 K.

percentage ratio spectral bathochromic shifts of ~25 nm (absorption) and ~15 nm (fluorescence) were observed Fig. 4 and Fig. 5. TPPS (5,10,15,20-tetrakis-(4-sulfonatophenyl)porphyrin) tetrasodium [47] was used for comparative purpose since its capability to form aggregates is well known [48,49].

Fluorescence quantum yields (ϕ_F) for the investigated compounds were obtained in solution and in the membranes. The fluorescence quantum yield of TMePyP decrease from 0.09 in DMSO solution to 0.011 in SPEEK film loaded with 0.10% of TMePyP; 0.008 in SPEEK film loaded with 0.20% of TMePyP and 0.006 in SPEEK film loaded with 0.30% of TMePyP. However, the fluorescence quantum yield of TPPS was not significantly changed going from solution (0.15) to the film (0.16).

Table 2 presents the fluorescence lifetimes collected with excitation at 451 nm in DMSO solution and in the membranes with 0.1% porphyrin to polymer loading. For $TMePyPI_4$ the decays in solution were found to be well fitted with a biexponential decay law (see Table 2). For TPPS instead a monoexponential decay was found, $\tau_F = 11.8$ ns, in agreement to what was previously reported [35]. Going on to membranes with 0.1% porphyrin loading, for $TMePyPI_4$ the fluorescence decays were only properly adjusted with a sum of three exponential terms: i) a shorter lifetime in the 0.25–0.29 ns range; ii) an intermediate lifetime of 1.4 ns; and iii) a longer fluorescence lifetime of 10.5–10.7 ns. The values are in good agreement with the those reported by Carbone *et. al.* [21], in which the longest decay time is attributed to the emission of the porphyrin monomeric form, the intermediary decay time to J-dimers emission and, finally, the fastest decays assigned to the emission of J-aggregates. In general, the Soret band hypsochromic shift, the decrease in fluorescence intensity [50] and the analysis of the fluorescence lifetimes indicate formation of J-type aggregates or dimers in the SPEEK composites.

To further investigate the excited state dynamics of the investigated porphyrins in solution and immobilized in SPEEK films the time-resolved transient absorption (TA) spectra were obtained in time-window of 7.6 ns (see Fig. 6). The spectra show, in the 450–800 nm range, dominating positive and broad transient absorption band(s) together with a negative transient absorption band (at *ca.* 420 nm in DMSO solution and in the 420–460 nm in the SPEEK films). This last band is in agreement with the ground state absorption (GSA) spectra shown in (Figs. 4 and 6).

3.4. Transient absorption (TA) data

The global analysis of the TA data of the TPPS and $TMePyPI_4$ porphyrins in aerated DMSO solutions shows: i) a fast decay transient lifetime of 1 ps; followed by ii) an intermediate decay with values of 105 ps and 23 ps, respectively; a iii) transient lifetimes of 10 ns (which match those found for the fluorescence lifetime of TPPS and of 2.8 ns for TMePyPI4; and finally iv) long lived transients which, in agreement with the observed sensitization of molecular singlet oxygen and to what was previously reported for meso-substituted porphyrins, was therefore fixed in the analysis and associated to the triplet excited state lifetimes (420 μs and 170 μs, respectively) [31,32,51]. Indeed, with excitation at the Soret band (450 nm), it is expected that for TPPS and $TMePyPI_4$ the time evolution of the TA bands shows, at different wavelengths, different profiles mirroring the various occurring processes. These include ground-state bleaching (GSB) and excited-state absorption relative to the $S_2 \rightarrow Sn$, $Q_y \rightarrow S_n$, $Q_x \rightarrow S_n$ and $T_1 \rightarrow T_n$ transitions that occur occur after photoexcitation [51]. Therefore, following excitation to S_2 the decay processes are essentially governed by internal conversion (IC), 1 ps, which populates S_1 (Q_y and Q_x bands) which is then followed by intersystem crossing (ISC) to the lowest triplet state T_1, and further decay of the T_1 state (which at room temperature is essentially radiationless). In the case of copper metalloporphyrin, as previously reported for open 3d shell metalloporphyrins after Soret band excitation the singlet excited state, $^2S_1$, undergoes rapid intersystem-crossing to the triplet excited state, $^2T_1$, which then populates the CT-excited state or decay with short transient lifetime [52,53].

The TA data analysis for the porphyrins immobilized in SPEEK films (0.1% loading) showed: i) for TPPS the kinetics were well fitted with a

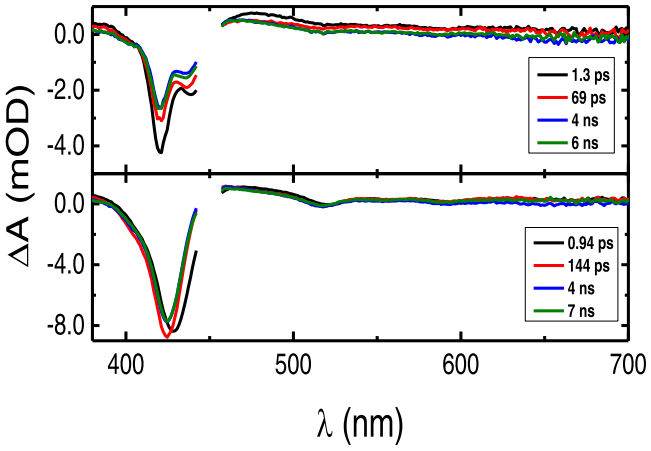

Fig. 6. Time resolved transient absorption spectra obtained for the TPPS and $TMePyPI_4$ porphyrins in DMSO at T = 293 K collected with excitation at 450 nm.

Table 2
Fluorescence lifetimes for the investigated porphyrins in DMSO solution and immobilized in SPEEK films (0.1% porphyrin to polymer loading).

Compd		λ_{em} (nm)	τ_1 (ns)	τ_2 (ns)	τ_3 (ns)	a_{i1}	a_{i2}	a_{i3}	χ^2
TPPS	DMSO Film (0.1%)	650			11.8				1.11
		665		3.4	5.8		0.487	0.513	1.07
		725					0.568	0.432	1.11
$TMePyPI_4$	DMSO Film (0.1%)	650		5.4	12.3				1.06
		665	0.25	1.4	10.5	0.641	0.308	0.078	1.13
		725				0.545	0.291	0.164	1.22

Table 3
Bulk resistivity (ρ_b) and proton conductivity (σ) of SPEEK-based membranes with different percentages of water uptake (H_p), at 25 °C.

	H_p / %	ρ_b / (10^5 cm/S) wet, RT	σ (mS/cm) wet, RT
SPEEK	51 (±7)	1.3 (±0.4)	30 (±4)
SPEEK/TMePyPI$_4$ 0.1%	33 (±5)	18.2 (±2.7)	27 (±3)
SPEEK/TMePyPI$_4$ 0.2%	30 (±3)	17.5 (±1.8)	31 (±2)
SPEEK/TMePyPI$_4$ 0.3%	30 (±6)	16.4 (±0.9)	29 (±0)
SPEEK/CuTMePyPI$_4$ 0.1%	24 (±9)	22.6 (±3.3)	34 (±0)
SPEEK/CuTMePyPI$_4$ 0.2%	34 (±14)	19.9 (±0.4)	26 (±2)
SPEEK/CuTMePyPI$_4$ 0.3%	32 (±8)	16.6 (±1.2)	31 (±1)

sum of three exponential terms, and lifetimes of 633 fs, 3.1 ns and, a long lifetime of 420 μs (fixed in the analysis and associated to the essentially radiationless decay of the triplet state in solution; and ii) for TMePyPI$_4$ four lifetimes were necessary to properly fit the kinetic traces, a shorter lifetime of 38 ps, a second decay component of 374 ps, a third of 3.7 ns and a long decay component that again was fixed to the triplet decay time obtained in solution 170 μs;.

Following photolysis of oxygen containing DMSO solutions of the porphyrins, the singlet oxygen formation quantum yields (ϕ_Δ) were obtained from the measurement of the molecular oxygen phosphorescence at 1270 nm. The ϕ_Δ values were further obtained with a plot of the initial phosphorescence intensity (observed at 1270 nm) as a function of the laser energy or doses. The comparison of the slope obtained for the studied porphyirins with that of the standard tetraphenylporphyrin in toluene provided the ϕ_Δ values. Furthermore, observing the obtained data, a marked decrease is observed in the ϕ_Δ values on going from TPPS (ϕ_Δ = 0.66 in toluene) to the methyl-pyridyl meso-porphyrins (0.16–0.17). Moreover and considering that, ϕ_Δ values cannot be higher than the quantum yield of triplet formation (that is $\phi_\Delta \leq \phi_T$) and assuming an efficient energy transfer from the triplet state of the meso-porphyrins to the triplet molecular oxygen ground-state, $S_\Delta = \phi_\Delta / \phi_T = 1$, it can be concluded that, in general, the non-radiative deactivation yields ($\phi_{IC} + \phi_T$) are the dominant deactivation pathways. Moreover, it can be seen that for TPPS ISC dominates the deactivation of S_1m, which contrasts with the methyl-pyridyl porphyrins derivative, TMePyPI$_4$, where IC is the dominant decay process (ϕ_{IC} in the 0.74). This feature could be related to the chemical stability of the SPEEK composites, the reduce ability to generate ROS will reduce the possibility of oxidation process to occur.

3.5. Electrical conductivity

Table 3 shows the dependence of the bulk resistivity (ρ_b) and proton conductivity (σ) on the composition of composite membranes. In general, it can be assessed that the incorporation of neat and Cu(II)-containing porphyrins leads to an increase, in one order of magnitude, of the bulk electrical resistivity but no significant alteration of proton conductivity was observed.

Since the water inside of membrane is of crucial importance for the current transport, the percentage of water uptake of the prepared membranes was measured. The results will be compared with those obtained for Nafion 115. Taking into account the experimental error the H_p of composite membranes are, in average, *ca.* 40% lower than the value for SPEEK membranes; such decrease can be justified by some phase separation detected by thermogravimetric analysis and may also justify the increase in the ρ_b values. This is also supported by photophysics analysis, where the presence of porphyrin aggregates was observed and for the HCl permeation (see following sections). However, it is worth noticing that an increase in the percentage of porphyrins into membranes, either as neat or Cu(II) complex, leads to a slight decrease in the ρ_b values, being more effective for the Cu(II)-containing porphyrin. The former may be justified by the interactions between porphyrins and sulfonate groups; however, by increasing the amount of porphyrins incorporated into membrane the interactions TMePyP-TMePyP becomes predominant leading to a more sulfonate groups free for conduction.

Table 4
Permeability, diffusivity and Henry's constant at 25 °C of HCl (0.1 M) in SPEEK-based membranes.

	D / (10^{-10} cm^2/s)	P / (10^{-11} cm^2/s)	K
SPEEK	6.1 (± 0.3)	9.3 (± 0.2)	0.15 (± 0.07)
SPEEK/TMePyPI$_4$ 0.1%	2.2 (± 0.6)	6.0 (± 1.2)	0.27 (± 0.09)
SPEEK/TMePyPI$_4$ 0.2%	3.0 (± 0.3)	6.2 (± 0.5)	0.20 (± 0.03)
SPEEK/TMePyPI$_4$ 0.3%	5.0 (± 1.1)	6.5 (± 1.1)	0.13 (± 0.04)
SPEEK/CuTMePyPI$_4$ 0.1%	3.5 (± 0.6)	7.5 (± 0.9)	0.21 (± 0.01)
SPEEK/CuTMePyPI$_4$ 0.2%	4.4 (± 0.6)	9.4 (± 0.9)	0.21 (± 0.04)
SPEEK/CuTMePyPI$_4$ 0.3%	7.6 (± 0.8)	10.9 (± 0.6)	0.12 (± 0.01)

However, the proton transport channels should also be affected with a decrease in the H_p [44,54], *i.e.*, the proton conductivity should also decrease. Consequently, it seems that the incorporation of porphyrins makes a balance between a decrease in the water uptake and an increase in the proton conductivity.

In order to check the effect of porphyrins on the electrical conductivity of SPEEK-based films, the results were compared with those obtained with Nafion 115 membrane. The obtained values for ρ_b and σ are: 2.4 (± 0.4) 10^5 cm/S and 93 (± 1) mS/cm, respectively. These values are similar to those reported elsewhere [55].

3.6. Permeation analysis

The permeation of HCl through membranes were carried out using a steady-state method to have an insight on the mechanism of proton conduction [28]. From Table 4, which summarizes the permeability, diffusivity and Henry's constant at 25 °C of HCl (0.1 M) in SPEEK-based membranes, we can conclude that the porphyrins affect essentially the HCl diffusivity. The diffusion coefficient of HCl inside SPEEK membranes is five orders of magnitude lower than the corresponding intermolecular diffusion coefficient of HCl (0.1 M) in water (3.017×10^{-5} cm^2/s [56]), which might be justified by the interaction between H_3O^+ and the SPEEK membrane, with consequent protonation of the SPEEK at specific sites – the sulfonate groups. It can also be stressed that the tortuosity might also explain the low effective diffusion coefficient; however, according to Cussler, this can only justify a variation in D value in one order of magnitude [57]. The diffusion coefficient of HCl in Nafion-115 membrane has been obtained and is equal to 5.82 (± 0.08) $\times 10^{-9}$ cm^2/s. This value is one half that D reported for the permeation of acetic acid (0.1 M) through Nafion 117 membranes (1.5×10^{-8} cm^2/s) [58] and of the same order of magnitude of the diffusion coefficient of HCl inside Nafion-117 as reported Schwitzgebel and Endres [59]. From this comparison it can be stated that the SPEEK-based membranes show a higher affinity towards H_3O^+ than the Nafion membranes. Such affinity towards hydronium seems to be enhanced by a lower percentage of water uptake in hybrid membranes.

Concerning the permeability coefficients, it can be concluded that the values only slightly change with the addition of porphyrins and its concentrations; even so, there is a trend for both composites: the P is lower for the composite with less amount of porphyrin and increase as the amount of porphyrin increases; this is in close agreement with the hypothesis of porphyrin aggregation and consequent occurrence of

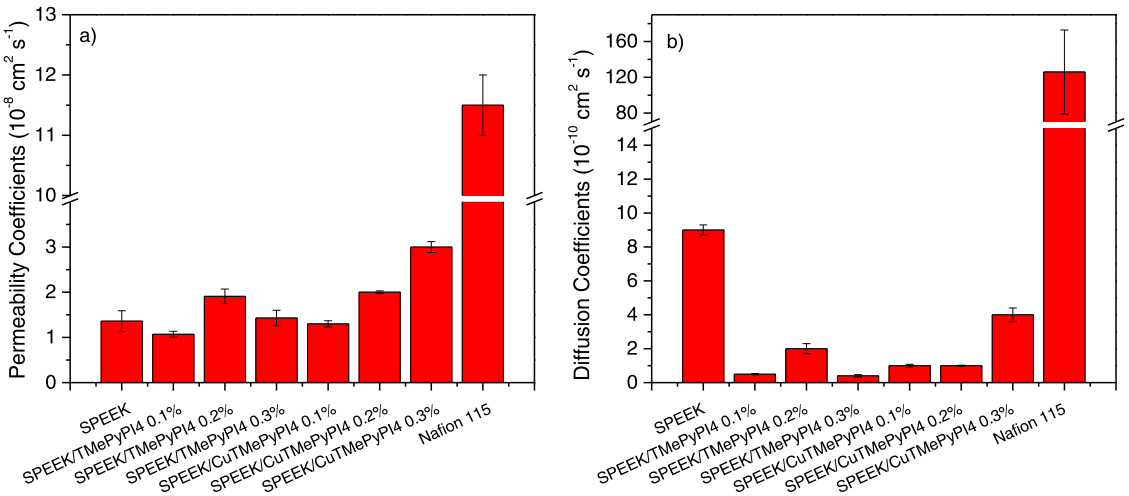

Fig. 7. Permeability and diffusion coefficients of VO^{2+} through SPEEK-based membranes; the results are compared with those obtained for Nafion 115.

phase separation [60].

The analysis of Henry's coefficients shows an enhancement of the proton transport channels in the presence of porphyrins.

As stated before, a drawback of Nafion membranes is the high crossover of vanadium ions, due to its low affinity, leading to short term operation and battery self-discharge when stored [61,62]. To evaluate the performance of the prepared membranes in such conditions, the flux of VO^{2+} through SPEEK membranes, in a H_2SO_4 aqueous medium, was measured and the results are shown in Fig. 7. In the present case, the use of sulfuric acid in both cells allows to decrease the contribution of the osmotic pressure for the flux of vanadium[63]. The analysis of Fig. 7 allows to withdraw the following conclusions: i) the permeability of SPEEK/TMePyPI$_4$ 0.1% membrane to V(IV) is the lowest, it is *ca.* eleven times lower than the permeability of Nafion 115; and ii) the diffusion coefficients of VO^{2+} in SPEEK/TMePyPI$_4$ 0.1% and SPEEK/CuTMePyPI$_4$ 0.1% are two and one order of magnitude lower than those observed for Nafion and SPEEK, respectively. Another interesting point is related with the effect of the membranes' hydrophilicity on the transport properties. Although there is no straight relationship between H_p and P or D for VO^{2+}, we can observe, as a general trend, a decrease of $K(VO^{2+})$ by increasing H_p, probably due to some competition with H_3O^+ provided by the sulfuric acid.

4. Conclusions

The use of SPEEK-based membranes for RFB has been revisited. SPEEK composites were prepared by addition of water soluble 5,10,15,20-*tetrakis*(N-methyl-4-pyridinyl)porphyrin iodide and its copper(II) complex. In line with the environmental concerns that motivate the development of fuel cells and RFBs, the organic compounds were prepared accordingly to Green Chemistry principles. The composites prepared showed a good thermal stability and chemical stability enhanced by the low capability of the copper porphyrin to produce reactive oxygen species. Weak self-aggregation of the water-soluble porphyrin and its copper complex, showed to be beneficial for stabilizing the morphology, leading to composites with homogeneous profile and featureless non-porous surface.

SPEEK loaded with water soluble cationic porphyrin presented low proton crossover and lower vanadium crossover. Despite that these membranes significantly decreases vanadium diffusion, proton crossover also decreased when compared with SPEEK free-based ones. However, the introduction of copper into the porphyrin core had a positive effect in both parameters, recovering the original proton diffusion and permeability of SPEEK and keeping low vanadium crossover values. Comparing with Nafion 115 membranes, SPEEK showed better performance in all measured properties, with the exception of proton and electrical conductivities. Additionally the selectivity VO^{2+}/H^+ increase significantly for porphyrin-containing SPEEK composites compared with both SPEEK and Nafion-115 membranes. Overall, the new SPEEK-based composites showed good mass transport properties, which together with the high thermal and chemical stability and the low cost make them an alternative candidate for the development of viable technologies to provide cleaner and more efficient sources of energy.

CRediT authorship contribution statement

Joana Sousa: Methodology, Formal analysis, Investigation, Writing – original draft. **João Pina:** Methodology, Formal analysis, Investigation, Writing – original draft. **Carla Gomes:** Formal analysis, Investigation. **Lucas D. Dias:** Methodology, Formal analysis, Investigation. **Mariette Pereira:** Conceptualization, Resources, Writing – review & editing. **Dina Murtinho:** Conceptualization; Methodology, Investigation, Writing – original draft, Writing – review & editing, Supervision. **Paula Dias:** Methodology, Formal analysis, Investigation, Writing – original draft. **João Azevedo:** Methodology, Formal analysis. **Adélio Mendes:** Conceptualization, Validation, Resources, Writing – review & editing, Supervision, Project administration. **J. Sérgio Seixas de Melo:** Conceptualization, Validation, Resources, Writing – review & editing, Supervision, Project administration. **Alberto Pais:** Conceptualization, Validation, Writing – review & editing, Supervision. **Marta Pineiro:** Conceptualization, Validation, Resources, Writing – original draft, Writing – review & editing, Supervision. **Artur Valente:** Conceptualization, Validation, Resources, Writing – original draft, Writing – review & editing, Supervision, Project administration.

Declaration of Competing Interest

The authors declare that they have no known competing financial interests or personal relationships, that could have appeared to influence the work reported in this paper.

Acknowledgements

This work was supported by Projects "Hylight" (no. 031625/02/SAICT/2017, PTDC/QUI-QFI/31625/2017, which is funded by the Portuguese Science Foundation and Compete Centro 2020 (Portugal), Project Suprasol (LISBOA-01-0145-FEDER-028365 -PTDC/QUI-QOR/28365/2017), funded by Fundo Europeu de Desenvolvimento Regional (FEDER), through Programa Operacional Regional Lisboa (LISBOA2020, Portugal), and project "SunStorage - Harvesting and storage of solar

energy" for financial support, reference POCI-01-0145-FEDER-016387, funded by FEDER, through COMPETE 2020 – Operational Programme for Competitiveness and Internationalization (OPCI), and by national funds, through Fundação para a Ciência e a Tecnologia (FCT) and Portuguese Agency for Scientific Research (Portugal). We acknowledge funding by Fundo Europeu de Desenvolvimento Regional (FEDER) through Programa Operacional Factores de Competitividade (COMPETE). L.D. Dias thanks FAPESP (Brazil) for the Post-doc grant 2019/13569-8, J. Azevedo would like to acknowledge the Portuguese Foundation for Science and Technology (FCT, Portugal) for funding (CEECIND/03937/2017) and P. Dias is grateful to FCT her individual contract (CEECIND/02862/2018). C. Gomes thanks FCT (Portugal) for PhD grant FCT- CATSUS PhD Program (PD/BD/135531/2018. The Coimbra Chemistry Centre is supported by the FCT, through Projects UIDB/00313/2020 and UIDP/00313/2020 and CQE is supported by FCT through project UID/QUI/00100/2019. LEPABE has also received funding from: i) Project PTDC/EQU-EQU/30760/2017 – HopeH2, Efficient, stable and scalable PEC-PV device for solar hydrogen generation - POCI-01-0145-FEDER-030760; and (ii) Project PTDC/EQU-EQU/30510/2017 – SunFlow, Solar energy storage into redox flow batteries - POCI-01-0145-FEDER-030510, both funded by the European Regional Development Fund (ERDF), through COMPETE2020 - Operational Programme for Competitiveness and Internationalisation (OPCI, Portugal) and by national funds, through FCT.

References

[1] A.C. Fernandes, E.A. Ticianelli, A performance and degradation study of Nafion 212 membrane for proton exchange membrane fuel cells 193 (2009) 547–554, https://doi.org/10.1016/j.jpowsour.2009.04.038.

[2] H. Tang, S. Peikang, S. Ping, F. Wang, M. Pan, A degradation study of Nafion proton exchange membrane of PEM fuel cells 170 (2007) 85–92, https://doi.org/10.1016/j.jpowsour.2007.03.061.

[3] C. Menictas, M. Skyllas-Kazacos, T. Lim, Advances in batteries for medium and large-scale energy storage, Elsevier (2015), https://doi.org/10.1016/C2013-0-16429-X.

[4] J. Kaldellis (Ed.), Stand-Alone and Hybrid Wind Energy Systems, Woodhead Publishing, Cambridge, 2010.

[5] P. Xing, G.P. Robertson, M.D. Guiver, S.D. Mikhailenko, K. Wang, S. Kaliaguine, Synthesis and characterization of sulfonated poly(ether ether ketone) for proton exchange membranes, J. Memb. Sci. 229 (2004) 95–106, https://doi.org/10.1016/j.memsci.2003.09.019.

[6] M.B. Karimi, F. Mohammadi, K. Hooshyari, Recent approaches to improve Nafion performance for fuel cell applications: a review, Int. J. Hydrog. Energy 44 (2019) 28919–28938, https://doi.org/10.1016/j.ijhydene.2019.09.096.

[7] Y. Liu, Y. Li, Y. Chen, T. Qu, C. Shu, X. Yang, H. Zhu, S. Guo, S. Zhao, T. Asefa, Y. Liu, A CO_2/H2 fuel cell: reducing CO 2 while generating electricity, J. Mater. Chem. A. 8 (2020) 8329–8336, https://doi.org/10.1039/D0TA02855J.

[8] T.M. Lim, M. Ulaganathan, Q. Yan, Advances in membrane and stack design of redox flow batteries (RFBs) for medium- and large-scale energy storage, Adv. Batter. Mediu. Large-Scale Energy Storage, Elsevier (2015) 477–507, https://doi.org/10.1016/B978-1-78242-013-2.00014-5.

[9] S. He, Y. Lin, H. Ma, H. Jia, X. Liu, J. Lin, Using ethanol / water mixed solvent, Mater. Lett. 169 (2016) 69–72, https://doi.org/10.1016/j.matlet.2016.01.099.

[10] M. Jun, Y. Choi, J. Kim, Solvent casting effects of sulfonated poly (ether ether ketone) for polymer electrolyte membrane fuel cell 396 (2012) 32–37, https://doi.org/10.1016/j.memsci.2011.12.008.

[11] Xiao Dhanapal, Meng Wang, A review on sulfonated polymer composite/organic-inorganic hybrid membranes to address methanol barrier issue for methanol fuel cells, Nanomaterials 9 (2019) 668, https://doi.org/10.3390/nano9050668.

[12] S. Sonpingkam, D. Pattavarakorn, Mechanical properties of sulfonated poly (ether ether ketone) nanocomposite membranes, Int. J. Chem. Eng. Appl. 5 (2014) 181–185, https://doi.org/10.7763/IJCEA.2014.V5.374.

[13] H. Hou, B. Maranesi, M. Khadhraoui, P. Knauth, R. Polini, M.L.Di Vona, Properties of composite membranes of SPEEK and nanodiamond, MRS Proc. 1384 (2012), https://doi.org/10.1557/opl.2012.188.

[14] S. Gahlot, P.P. Sharma, P.K. Jha, V. Kulshrestha, CNT/SPEEK nano-composite membranes: toward improved properties, Macromol. Symp 376 (2017) 170048, https://doi.org/10.1002/masy.201700048.

[15] W. Dai, Y. Shen, Z. Li, L. Yu, J. Xi, X. Qiu, SPEEK/Graphene oxide nanocomposite membranes with superior cyclability for highly efficient vanadium redox flow battery, J. Mater. Chem. A. 2 (2014) 12423–12432, https://doi.org/10.1039/C4TA02124J.

[16] S.-W. Kim, S.-Y. Choi, H.-W. Rhee, Sulfonated poly(etheretherketone) based nanocomposite membranes containing POSS-SA for polymer electrolyte membrane fuel cells (PEMFC), J. Memb. Sci. 566 (2018) 69–76, https://doi.org/10.1016/j.memsci.2018.08.040.

[17] Y. Kozawa, S. Suzuki, M. Miyayama, T. Okumiya, E. Traversa, Proton conducting membranes composed of sulfonated poly(etheretherketone) and zirconium phosphate nanosheets for fuel cell applications, Solid State Ion. 181 (2010) 348–353, https://doi.org/10.1016/j.ssi.2009.12.017.

[18] X. Liu, J. Zhou, M. Meng, G.Y. Zhu, Y. Tan, X. Chen, J. Wei, D.B. Kuang, Y.Y. Wu, S. Su, T. Cheng, Y. Zhou, C.Y. Liu, A Mo2-ZnP molecular device that mimics photosystem I for solar-chemical energy conversion, Appl. Catal. B: Environ. 286 (2021), 119836, https://doi.org/10.1016/j.apcatb.2020.119836.

[19] J. Zhang, D. Zhong, T. Lu, Co(II)-based molecular complexes for photochemical CO_2 reduction, Acta Phys. Chim. Sin. 0 (2020), 2008068, https://doi.org/10.3866/PKU.WHXB202008068.

[20] Z. Li, E. Borguet, Determining charge transport pathways through single porphyrin molecules using scanning tunneling microscopy break junctions, J. Am. Chem. Soc. 134 (2012) 63–66, https://doi.org/10.1021/ja208600v.

[21] A. Carbone, M. Gaeta, A. Romeo, G. Portale, R. Pedicini, I. Gatto, M.A. Castriciano, Porphyrin/sPEEK membranes with improved conductivity and durability for PEFC technology, ACS Appl. Energy Mater. 1 (2018) 1664–1673, https://doi.org/10.1021/acsaem.8b00126.

[22] J. Lu, Z. Li, W. An, L. Liu, W. Cui, Tuning the supramolecular structures of metal-free porphyrin via surfactant assisted self-assembly to enhance photocatalytic performance, Nanomaterials 9 (2019) 1321, https://doi.org/10.3390/nano9091321.

[23] A. Carbone, A. Saccà, R. Pedicini, I. Gatto, E. Passalacqua, A. Romeo, L.M. Scolaro, M.A. Castriciano, Composite sPEEK-TPyP membranes development for portable applications, Int. J. Hydrog. Energy 40 (2015) 17394–17401, https://doi.org/10.1016/j.ijhydene.2015.07.159.

[24] S. Wang, M. Wang, Z. Chen, X. Yang, Selection strategy of porphyrins for achieving thermally stable polymer solar cells, J. Mater. Chem. A. 3 (2015) 21051–21059, https://doi.org/10.1039/C5TA05628D.

[25] C.-D. Si, X.-D. Lv, S.-J. Long, Perovskite solar cells employing copper (I/II) porphyrin hole-transport material with enhanced performance, Inorg. Chem. Commun. 112 (2020), 107701, https://doi.org/10.1016/j.inoche.2019.107701.

[26] C.M.R. Almeida, B.F.O. Nascimento, M. Pineiro, A.J.M. Valente, Thermodynamic study of the interaction between 5,10,15,20-tetrakis-(N-methyl-4-pyridyl) porphyrin tetraiodine and sodium dodecyl sulfate, Colloids Surf. A Physicochem. Eng. Asp. 480 (2015) 279–286, https://doi.org/10.1016/j.colsurfa.2014.12.030.

[27] A.J. Valente, H. Burrows, M. Miguel, V.M. Lobo, Diffusion coefficients of sodium dodecyl sulfate in water swollen cross-linked polyacrylamide membranes, Eur. Polym. J. 38 (2002) 2187–2196, https://doi.org/10.1016/S0014-3057(02)00125-8.

[28] A.J.M. Valente, A.Y. Polishchuk, V.M.M. Lobo, H.D. Burrows, Transport properties of concentrated aqueous sodium dodecyl sulfate solutions in polymer membranes derived from cellulose esters, Langmuir 16 (2000) 6475–6479, https://doi.org/10.1021/la000286l.

[29] L. Zhang, L. Ling, M. Xiao, D. Han, S. Wang, Y. Meng, Effectively suppressing vanadium permeation in vanadium redox flow battery application with modified Nafion membrane with nacre-like nanoarchitectures, J. Power Sources 352 (2017) 111–117, https://doi.org/10.1016/j.jpowsour.2017.03.124.

[30] D. Law, A. Blakeney, R. Tkachuk, The kubelka–munk equation: some practical considerations, J. Infrared Spectrosc. 4 (1996) 189–193, https://doi.org/10.1255/jnirs.89.

[31] S. Murov, I. Carmichael, L. Gordon, Handbook of Photochemistry, Marcel Dekker, New York, 1993.

[32] M. Pineiro, A.L. Carvalho, M.M. Pereira, A.M. d′A.R. Gonsalves, L.G. Arnaut, S. J. Formosinho, , Photoacoustic measurements of porphyrin triplet-state quantum yields and singlet-oxygen efficiencies, Chem. A Eur. J. 4 (1998) 2299–2307, https://doi.org/10.1002/(SICI)1521-3765(19981102)4:11<2299::AID-CHEM2299>3.0.CO;2-H.

[33] J.S. Seixas de Melo, J. Pina, F.B. Dias, A.L. Maçanita, Experimental techniques for excited state characterisation, in: Appl. Photochem., Springer, Netherlands, Dordrecht, 2013, pp. 533–585, https://doi.org/10.1007/978-90-481-3830-2_15.

[34] C.J.P. Monteiro, J. Pina, M.M. Pereira, L.G. Arnaut, On the singlet states of porphyrins, chlorins and bacteriochlorins and their ability to harvest red/infrared light, Photochem. Photobiol. Sci. 11 (2012) 1233–1238, https://doi.org/10.1039/c2pp25021g.

[35] G. Striker, V. Subramaniam, C.A.M. Seidel, A. Volkmer, Photochromicity and fluorescence lifetimes of green fluorescent protein, J. Phys. Chem. B. 103 (1999) 8612–8617, https://doi.org/10.1021/jp991425e.

[36] J. Pina, M.-J.R.P. Queiroz, J. Seixas de Melo, Effect of substitution on the ultrafast deactivation of the excited state of benzo[b]thiophene-arylamines, Photochem. Photobiol. Sci. 15 (2016) 1029–1038, https://doi.org/10.1039/C6PP00140H.

[37] B.F.O. Nascimento, A.M. d′A. Rocha Gonsalves, M. Pineiro, MnO_2 instead of quinones as selective oxidant of tetrapyrrolic macrocycles, Inorg. Chem. Commun. 13 (2010) 395–398, https://doi.org/10.1016/j.inoche.2009.12.032.

[38] M. Pineiro, Microwave-assisted synthesis and reactivity of porphyrins, Curr. Org. Synth. 11 (2014) 89–109, https://doi.org/10.2174/15701794113106660088.

[39] P.T. Anastas , J.C. Warner , Green Chemistry: Theory and Practice, Oxford University Press, New York, n.d.

[40] J.-H. Chang, J.H. Park, G.-G. Park, C.-S. Kim, O.O. Park, Proton-conducting composite membranes derived from sulfonated hydrocarbon and inorganic materials, J. Power Sources 124 (2003) 18–25, https://doi.org/10.1016/S0378-7753(03)00605-0.

[41] R. Jiang, H.R. Kunz, J.M. Fenton, Investigation of membrane property and fuel cell behavior with sulfonated poly(ether ether ketone) electrolyte: Temperature and relative humidity effects, J. Power Sources 150 (2005) 120–128, https://doi.org/10.1016/j.jpowsour.2005.03.180.

[42] J.-M. Song, J. Shin, J.-Y. Sohn, Y.C. Nho, Preparation and characterization of SPEEK membranes crosslinked by electron beam irradiation, Macromol. Res. 19 (2011) 1082–1089, https://doi.org/10.1007/s13233-011-1013-7.
[43] P. Knauth, H. Hou, E. Bloch, E. Sgreccia, M.L. Di Vona, Thermogravimetric analysis of SPEEK membranes: thermal stability, degree of sulfonation and cross-linking reaction, J. Anal. Appl. Pyrolysis 92 (2011) 361–365, https://doi.org/10.1016/j.jaap.2011.07.012.
[44] X. Liu, Z. Yang, Y. Zhang, C. Li, J. Dong, Y. Liu, H. Cheng, Electrospun multifunctional sulfonated carbon nanofibers for design and fabrication of SPEEK composite proton exchange membranes for direct methanol fuel cell application, Int. J. Hydrog. Energy 42 (2017) 10275–10284, https://doi.org/10.1016/j.ijhydene.2017.02.128.
[45] K. Lang, J. Mosinger, D.M. Wagnerová, Photophysical properties of porphyrinoid sensitizers non-covalently bound to host molecules; models for photodynamic therapy, Coord. Chem. Rev. 248 (2004) 321–350, https://doi.org/10.1016/j.ccr.2004.02.004.
[46] X. Yan, D. Holten, Effects of temperature and solvent on excited-state deactivation of copper(II) octaethyl- and tetraphenylporphyrin: relaxation via a ring-to-metal charge-transfer excited state, J. Phys. Chem. 92 (1988) 5982–5986, https://doi.org/10.1021/j100332a029.
[47] T. Carmona, M. Pineiro, C.J.P. Monteiro, M.M. Pereira, A.J.M. Valente, Interactions between cationic surfactants and 5,10,15,20-tetrakis(4-sulfonatophenyl)porphyrin tetrasodium salt as seen by electric conductometry and spectroscopic techniques, Colloids Surf. A: Physicochem. Eng. Asp. 481 (2015) 288–296, https://doi.org/10.1016/j.colsurfa.2015.05.025.
[48] L. Kelbauskas, S. Bagdonas, W. Dietel, R. Rotomskis, Excitation relaxation and structure of TPPS4 J-aggregates, J. Lumin. 101 (2003) 253–262, https://doi.org/10.1016/S0022-2313(02)00547-1.
[49] L.P.F. Aggarwal, I.E. Borissevitch, On the dynamics of the TPPS4 aggregation in aqueous solutions, Spectrochim. Acta Part A Mol. Biomol. Spectrosc. 63 (2006) 227–233, https://doi.org/10.1016/j.saa.2005.05.009.
[50] K. Šišková, B. Vlčková, P. Mojzeš, Spectral detection of J-aggregates of cationic porphyrin and investigation of conditions of their formation, J. Mol. Struct. 744–747 (2005) 265–272, https://doi.org/10.1016/j.molstruc.2004.10.047.
[51] Y. Venkatesh, M. Venkatesan, B. Ramakrishna, P.R. Bangal, Ultrafast time-resolved emission and absorption spectra of meso -Pyridyl porphyrins upon soret band excitation studied by fluorescence up-conversion and transient absorption spectroscopy, J. Phys. Chem. B. 120 (2016) 9410–9421, https://doi.org/10.1021/acs.jpcb.6b05767.
[52] D. Jeong, D. Kang, T. Joo, S.K. Kim, Femtosecond-resolved excited state relaxation dynamics of copper (II) tetraphenylporphyrin (CuTPP) after soret band excitation, Sci. Rep. 7 (2017) 16865, https://doi.org/10.1038/s41598-017-17296-z.
[53] V.S. Chirvony, M. Négrerie, J.-L. Martin, P.-Y. Turpin, Picosecond dynamics and mechanisms of photoexcited Cu(II)-5,10,15,20- m eso -tetrakis(4- N -methylpyridyl)porphyrin quenching by oxygen-containing lewis-base solvents, J. Phys. Chem. A. 106 (2002) 5760–5767, https://doi.org/10.1021/jp0134998.
[54] H. Namazi, H. Ahmadi, Improving the proton conductivity and water uptake of polybenzimidazole-based proton exchange nanocomposite membranes with TiO2 and SiO2 nanoparticles chemically modified surfaces, J. Power Sources 196 (2011) 2573–2583, https://doi.org/10.1016/j.jpowsour.2010.10.082.
[55] M.P. Rodgers, Z. Shi, S. Holdcroft, Ex situ characterisation of composite nafion membranes containing zirconium hydrogen phosphate, Fuel Cells 9 (2009) 534–546, https://doi.org/10.1002/fuce.200900027.
[56] V.M.M. Lobo, M. Helena, S.F. Teixeira, Diffusion coefficients in aqueous solutions of hydrochloric acid at 298 K, Electrochim. Acta 24 (1979) 565–567, https://doi.org/10.1016/0013-4686(79)85033-1.
[57] E.L. Cussler, Diffusion, Cambridge University Press, Cambridge, 2009, https://doi.org/10.1017/CBO9780511805134.
[58] R. Dugas, D. Guay, A.C. Tavares, Simultaneous determination of the permeability of a nafion membrane to formic acid and water, Fuel Cells 13 (2013) 1024–1031, https://doi.org/10.1002/fuce.201200228.
[59] G. Schwitzgebel, F. Endres, The determination of the apparent diffusion coefficient of HCl in Nafion®-117 and polypyrrole + Nafion®-117 by simple potential measurements, J. Electroanal. Chem. 386 (1995) 11–16, https://doi.org/10.1016/0022-0728(95)03797-K.
[60] A. Stolarczyk, R. Turczyn, A. Januszkiewicz-Kaleniak, W. Domagała, S. Imach, Determination and comparison of ideal and practical selectivity coefficients of membranes containing different conductive polymers, Acta Phys. Pol. A. 124 (2013) 563–566, https://doi.org/10.12693/APhysPolA.124.563.
[61] K. Shirasaki, T. Yamamura, Direct observation of vanadium ion permeation behavior through Nafion 117 using 48V radiotracer for all-vanadium redox flow battery, J. Membr. Sci. 592 (2019), 117367, https://doi.org/10.1016/j.memsci.2019.117367.
[62] H. Prifti, A. Parasuraman, S. Winardi, T.M. Lim, M. Skyllas-Kazacos, Membranes for redox flow battery applications, Membranes (2012) 275–306, https://doi.org/10.3390/membranes2020275.
[63] S. Kim, S. Yuk, H.G. Kim, C. Choi, R. Kim, J.Y. Lee, Y.T. Hong, H.T. Kim, A hydrocarbon/Nafion bilayer membrane with a mechanical nano-fastener for vanadium redox flow batteries, J. Mater. Chem. A. 5 (2017) 17279–17286, https://doi.org/10.1039/C7TA02921G.